The Mitochondrial Oxoglutarate Carrier: Structural and Dynamic Properties of Transmembrane Segment IV Studied by Site-Directed Spin Labeling[†,‡]

Blasco Morozzo della Rocca,[§] Graziantonio Lauria,[||] Francesca Venerini,[§] Luigi Palmieri,[||,⊥] Francesca Polizio,[§] Loredana Capobianco,[#] Valentina Stipani,[||] Jens Pedersen,[§] Anna Rita Cappello,[||] Alessandro Desideri,*[,§] and Ferdinando Palmieri*[,||]

INFM and Department of Biology, University of Rome "Tor Vergata", via della Ricerca Scientifica snc, 00133 Rome, Italy, Department of Pharmaco-Biology, Laboratory of Biochemistry and Molecular Biology, University of Bari, via Orabona 4, 70125 Bari, Italy, CNR Institute of Biomembranes and Bioenergetics, via Orabona 4, 70125 Bari, Italy, and Dipartimento di Scienze e Tecnologie Biologiche ed Ambientali, University of Lecce, via Monteroni, 73100 Lecce, Italy

Received October 17, 2002; Revised Manuscript Received February 26, 2003

ABSTRACT: The structural and dynamic features of the fourth transmembrane segment of the mitochondrial oxoglutarate carrier were investigated using site-directed spin labeling and electron paramagnetic resonance (EPR). Using a functional carrier protein with native cysteines replaced with serines, the 18 consecutive residues from S184 to S201 which are believed to form the transmembrane segment IV were substituted individually with cysteine and labeled with a thiol-selective nitroxide reagent. Most of the labeled mutants exhibited significant oxoglutarate transport in reconstituted liposomes, where they were examined by EPR as a function of the incident microwave power in the presence and absence of two paramagnetic perturbants, i.e., the hydrophobic molecular oxygen or the hydrophilic chromium oxalate complex. The periodicity of the sequence-specific variation in the spin-label mobility and the O_2 accessibility parameters unambiguously identifies the fourth transmembrane segment of the mitochondrial oxoglutarate carrier as an α-helix. The accessibility to chromium oxalate is out of phase with oxygen accessibility, indicating that the helix is amphipatic, with the hydrophilic face containing the residues found to be important for transport activity by site-directed mutagenesis and chemical modification. The helix is strongly packed, as indicated by the values of normalized mobility, which also suggest that the conformational changes occurring during transport probably involve the N-terminal region of the helix.

The mitochondrial oxoglutarate carrier (OGC)[1] catalyzes the transport of 2-oxoglutarate across the mitochondrial inner membrane in exchange for malate, or other dicarboxylates, and plays an important role in several metabolic processes (*1*, *2*). The OGC belongs to a large family of related transport proteins (see ref *3* and references therein). The primary structures of the family members are made up of three tandemly repeated homologous domains of about 100 amino acids in length, each containing a characteristic sequence motif and two hydrophobic stretches (*4*). The OGC has been shown to exist as a homodimer (*5*), each monomer being folded in the mitochondrial membrane into six transmembrane segments (*6*, *7*). In addition, the OGC has been the first eukaryotic membrane protein to be expressed in *Escherichia coli* and refolded in reconstitutively active state (*8*). More recently, Cys-scanning mutagenesis has been employed to examine the residues in transmembrane segment IV (TMSIV) and in part of the flanking hydrophilic loops (*9*). Within TMSIV of the OGC, two essential residues (R190 and Q198) and four engineered cysteines (T187C, A191C, V194C, and N195C) that bind thiol reagents with loss of function have been suggested to line a water-accessible crevice that is part of the substrate translocation pathway through the OGC protein (*9*). The importance of TMSIV in the transport process is also supported by indirect evidence that its N-terminal part is involved in the substrate-induced conformation change of the OGC protein (*10*).

Because of the lack of a general method for crystallizing membrane proteins, an alternative method to obtain information on the structure as well as on the functional dynamics of these proteins is site-directed spin labeling (SDSL) (*11*−*13*). This strategy involves the systematic introduction of a

[†] This work was supported by grants from MIUR-PRIN, CEGBA, and the CNR target project on Biotechnology and by the European Social Fund.

[‡] Dedicated to the memory of professor Eraldo Antonini.

* Corresponding authors. (F.P.) Address: Dipartimento Farmaco-Biologico, Università di Bari, via E. Orabona 4, 70125 Bari, Italy. Tel.: +39-080-5443374. Fax: +39-080-5442770. E-mail: fpalm@farmbiol.uniba.it. (A.D.) Address: Dipartimento di Biologia, Università di Roma "Tor Vergata", via della Ricerca Scientifica snc, 00133 Roma, Italy. Tel.: +39-06-72594376. Fax: +39-06-72594326. E-mail: desideri@bio.uniroma2.it.

[§] INFM and University of Rome "Tor Vergata".

[||] University of Bari.

[⊥] CNR.

[#] University of Lecce.

[1] Abbreviations: ASM, 4-acetamido-4′-maleimidylstilbene-2,2′-disulfonic acid; CrOx, potassium chromium oxalate; DTE, dithioerythritol; EPR, electron paramagnetic resonance; MTSEA, (2-aminoethyl)-methanethiosulfonate hydrobromide; MTSES, sodium (2-sulfonatoethyl)methanethiosulfonate; MTSET, [2-(trimethylammonium)ethyl]methanethiosulfonate; MTSL, (1-oxyl-2,2,5,5-tetramethyl-Δ3-pyrroline-3-methyl)methanethiosulfonate; NEM, *N*-ethylmaleimide; OGC, oxoglutarate carrier; PIPES, piperazine-*N*,*N*′-bis(2-ethanesulfonic acid); SDSL, site-directed spin labeling; SDS−PAGE, sodium dodecyl sulfate-polyacrylamide gel electrophoresis; TMSIV, transmembrane segment IV; Tris, tris(hydroxymethyl)aminomethane.

10.1021/bi027025q CCC: $25.00
Published on Web 04/05/2003

nitroxide side chain at a selected site, achieved by cysteine substitution mutagenesis followed by modification of the protein's sulfhydryl group with a selective nitroxide reagent. Nitroxide-scanning experiments provide sequence-correlated data that can identify regular secondary structures. Moreover, on the basis of nitroxide accessibility to hydrophilic and hydrophobic paramagnetic agents, information can be obtained on the local environment and the depth of immersion of the side chains in the bilayer. SDSL has been successfully applied to several systems such as bovine rhodopsin (*14*), the KcsA channel (*15, 16*), lactose permease from *E. coli* (*17*), and the mitochondrial citrate carrier (*18*).

In this work we have applied the SDSL approach to TMSIV of OGC, introducing MTSL at 18 consecutive residues from S184C to S201C and studying their relative mobility as well as their accessibility to molecular oxygen and potassium chromium oxalate (CrOx). Our results indicate that TMSIV is in an α-helical conformation and identify a face of the helix as solvated by the lipid bilayer. The opposite face is more hydrophilic and accessible to water-soluble compounds such as CrOx. Furthermore, a semiquantitave analysis of the mobility indicates that the TMSIV is a highly packed rigid helix with a somewhat higher degree of mobility at its N-terminus.

MATERIALS AND METHODS

Construction of Plasmids and Site-Directed Mutagenesis. The plasmids containing the cDNA of the bovine OGC mutant devoid of Cys residues (C-less OGC) or the cDNAs corresponding to single-Cys-replacement mutants of the C-less OGC (from S184C to S201C as well as F208C and Y259C) were obtained as previously described (*9*).

Overexpression and Purification of C-less OGC and Single-Cys OGC Mutants. The overproduction of OGC mutants as inclusion bodies in *E. coli* C0214(DE3) was performed as described before (*8*, *9*). Inclusion bodies were isolated as described previously (*8*), and the recombinant OGC mutants were extracted in the presence of 1% SDS and purified by SDS−PAGE performed according to Laemmli (*19*). The separation gel (20 × 20 × 0.3 cm) contained 17.5% acrylamide and an acrylamide/bis(acrylamide) ratio of 37.5 (30:0.8) to give a high resolution of polypeptides of an apparent molecular mass value close to 30 000 Da. Approximately 5 mg of inclusion body protein was loaded onto the gel, and two separate lanes at either side of the gel were loaded with molecular weight markers. After electrophoresis, lateral strips were cut from the gel and stained with Coomassie blue to identify the band corresponding to the OGC mutant. The band was excised from the gel and electroeluted for 4 h in a 422-type Electro-eluter (Bio-Rad, Milan, Italy) using a Tris-glycine-SDS buffer (25 mM Tris, 192 mM glycine and 0.1% (w/v) SDS). The buffer was then extensively exchanged with DM buffer (0.17 mM dodecylmaltoside, 1 mM EDTA and 10 mM Tris-HCl, pH 7.1) using Centricon-30 tubes flooded repetitively with excess DM buffer for about 36 h. The amount of recombinant protein was estimated from Coomassie blue-stained SDS−PAGE by the Bio-Rad GS-700 Imaging Densitometer equipped with the software Bio-Rad Multi-Analyst, using carbonic anhydrase as standard.

Spin Labeling of Single-Cys OGC Mutants. The recombinant proteins were incubated with DTE and, after removal of the reductant by size-exclusion chromatography on a Sephadex G-25 column, labeled with excess (1-oxyl-2,2,5,5-tetramethyl-Δ3-pyrroline-3-methyl)methanethiosulfonate (MTSL), a paramagnetic probe that reacts selectively with Cys residues. The unreacted label was removed by gel-filtration on an FPLC apparatus with a Fast Desalting column HR 10/10 (Amersham-Pharmacia, Milan, Italy) eluted with DM buffer. Protein was concentrated to about 10 mg/mL using Centricon 30 tubes (Amicon, Milan, Italy) and analyzed by EPR spectroscopy. The spectra of the proteins in DM are those of a noninteracting spin label having a mobility intermediate between that of a completely free and a fully immobilized label, indicating that the proteins were not aggregated.

Reconstitution of OGC Mutants into Liposomes and Transport Measurements. Labeled recombinant proteins were reconstituted into artificial phospholipid vesicles as described previously (*9*, *20*). The reconstitution mixture consisted of DM-solubilized protein (about 500 or 10 μg, for EPR measurements or functional assays, respectively), 10 mg of Triton X-114, 10 mg of egg-yolk phospholipids (Fluka, Milan, Italy) as sonicated liposomes, 30 mM oxoglutarate, 10 mM PIPES, pH 7.0, and water (final volume 700 μL). The mixture was recycled 13 times through an Amberlite column (3.2 cm × 0.5 cm) pre-equilibrated with buffer containing 30 mM oxoglutarate and 10 mM PIPES, pH 7.0. All operations were performed at 4° C, except the passages through Amberlite, which were carried out at room temperature. The amount of protein incorporated into liposomes was determined as described in Phelps et al. (*21*); in all cases incorporated protein was between 15 and 20% of the protein added to the reconstitution mixture. The external substrate was removed from proteoliposomes on a Sephadex G-75 gel filtration column, pre-equilibrated with buffer A (50 mM NaCl and 10 mM PIPES, pH 7.0). The eluted proteoliposomes were either pelleted at 110 000*g* for 90 min at 4 °C and resuspended in a minimal volume of supernatant for EPR measurements, or used directly for functional assays. Transport at 25 °C was started by adding [^{14}C]oxoglutarate to proteoliposomes and terminated by the addition of 20 mM pyridoxal 5′-phosphate and 20 mM bathophenanthroline (the inhibitor-stop method, *20*). Entrapped radioactivity was counted (*20*). The experimental values were corrected by subtracting control values, and the transport activities were calculated by taking into account the efficiency of reconstitution (i.e., the share of successfully incorporated protein).

EPR Measurements. EPR spectra were recorded as first derivative spectra on a Bruker ESP 300 spectrometer equipped with a loop gap resonator using 1.0 G modulation at room temperature. Spin concentration as evaluated by double integration of the signal compared to that of a standard label solution was of the order of 10^{-5} M. The line width (ΔH) of each spectrum was evaluated as the peak-to-peak center line width using the Bruker EPR software. The scaled mobility (M_s) is defined as $M_s = (\Delta H^{-1} - \Delta H_i^{-1})/(\Delta H_m^{-1} - \Delta H_i^{-1})$, where ΔH is the width of the central resonance line of the spin label at the site of interest, ΔH_i is the corresponding width of the most immobilized MTSL, and ΔH_m is the corresponding width of the most mobile MTSL (*11*).

Power saturation experiments, from 0.2 up to 200 mW incident power, were carried out under a nitrogen atmo-

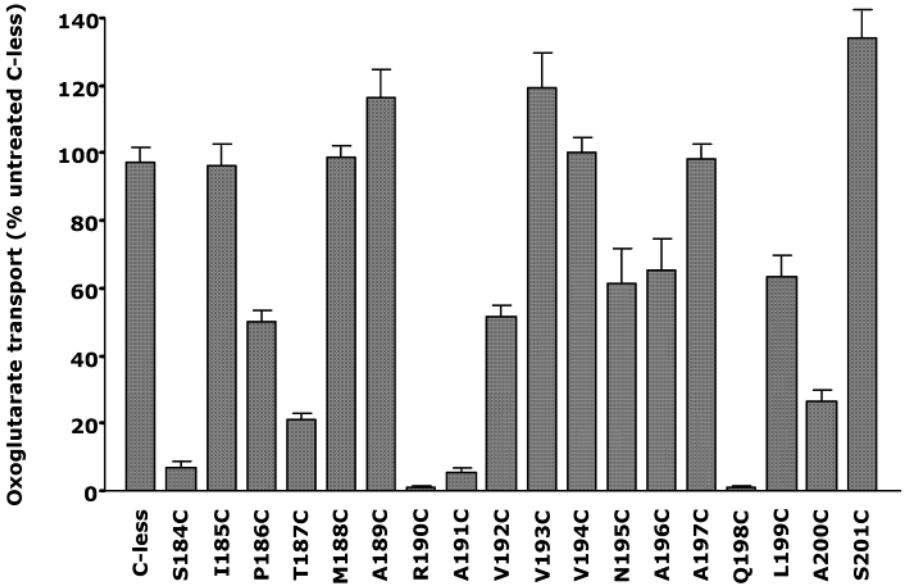

FIGURE 1: Steady-state levels of oxoglutarate transport by reconstituted single-Cys OGC mutants or C-less OGC treated with MTSL. The single-letter amino acid code along the horizontal axis denotes the residues of the C-less OGC replaced with Cys. Proteoliposomes were reconstituted with the indicated single-Cys OGC mutants and the C-less OGC treated with MTSL. Transport was started by the addition of 3 mM [^{14}C]oxoglutarate and terminated after 90 min. The values of oxoglutarate transport are expressed as a percentage of the MTSL-untreated C-less OGC value, which was 8635 ± 1215 nmol (mg protein)$^{-1}$. The data represent means ± S.D. of at least three independent experiments in duplicate.

sphere, in the presence of oxygen or in the presence of 30 mM potassium chromium oxalate in equilibrium with nitrogen; equilibration with the gaseous atmosphere was guaranteed by TPX capillaries as sample holders. Power saturation curves were obtained from the peak-to-peak amplitude of the central line of the EPR spectra and plotted as a function of the square root of the incident power. The parameter, $P_{1/2}$, corresponding to the microwave power at which the peak-to-peak amplitude is half saturated, was extracted upon curve fitting as shown in Figure 4, using the equation $A = I[1+ (2^{-\epsilon} - 1)(P/P_{1/2})]^{-\epsilon}\sqrt{P}$, where A is the measured amplitude of the EPR signal, P is the incident power, I is a scaling factor, and ϵ is a factor related to the homogeneity of the line (*13, 22*). Three sets of values were generated in this way corresponding to different experimental conditions: in equilibrium with nitrogen (as reference), in equilibrium with air (20% oxygen), and in the presence of 30 mM potassium chromium oxalate in equilibrium with nitrogen. The difference, $\Delta P_{1/2}$, between the values of the half saturation parameter measured in the presence and absence of paramagnetic perturbants, was used to calculate the dimensionless accessibility parameters ΠO_2 and ΠCrOx using the formula $\Pi = [\Delta P_{1/2}/\Delta H]/[P_{1/2}(\text{DPPH})/\Delta H(\text{DPPH})]$, where $P_{1/2}$(DPPH) and ΔH(DPPH) are the half-saturation power and the spectrum line width of DPPH (2,2-diphenyl-1-picrylhydrazyl) used as standard, respectively (*13, 22*).

The resultant vectors shown in Figure 5 were obtained by the vectorial sum of the CrOx accessibility and O_2 accessibility data reported in Figure 3 and of the mobility parameter ΔH^{-1} data, individually plotted as vectors starting from the center of the helix wheel representing TMSIV of OGC and pointing toward the respective residue.

ASM Labeling of Single-Cys OGC Mutants. Proteoliposomes reconstituted with the recombinant F208C or Y259C OGC mutant were incubated with 20 μM 4-acetamido-4′-maleimidylstilbene-2,2′-disulfonic acid for 1 h at 25 °C, and the reaction was stopped by adding 10 mM DTE. After treatment with ASM, the proteoliposomes were passed through a Sephadex G-75 column, pre-equilibrated with buffer A, and precipitated with a 20-fold excess of cold acetone for 4 h at −20 °C. The sample was centrifuged at 44 000*g* for 10 min at 0 °C. The lipids were removed essentially as described by Wessel and Flugge (*23*). Then, the recombinant protein was subjected to SDS−PAGE and to fluorographic analysis (*10*).

RESULTS AND DISCUSSION

Purification of OGC mutants. For accurate analysis of the EPR spectra, no spurious signal should be present in the spectra. Using the purification procedure employed in our previous studies, each OGC mutant was more than 90% pure (*9*). However, in preliminary experiments carried out with the C-less OGC, we found that the spin label reacted with minor contaminants. Therefore, an alternative procedure of purification and reconstitution of the OGC mutants was developed. The recombinant proteins were purified from isolated inclusion bodies by SDS−PAGE to homogeneity and, after exchange of SDS with dodecyl-maltoside, were reconstituted into liposomes. In the reconstituted system, all the OGC mutants used in this study showed an oxoglutarate transport activity comparable to that of the same proteins purified from inclusion bodies with the standard procedure (*8, 9*).

Effect of the Spin Label on the Activity of OGC Mutants. Eighteen single-Cys mutants from S184C to S201C of the mitochondrial C-less OGC were labeled with MTSL, reconstituted into liposomes, and their activities were investigated. These residues form the OGC TMSIV, which was suggested to be important within the OGC protein for the substrate translocation mechanism (*9*). The steady-state levels of oxoglutarate transport are reported in Figure 1 for each of the spin-labeled mutants as a percentage of the untreated

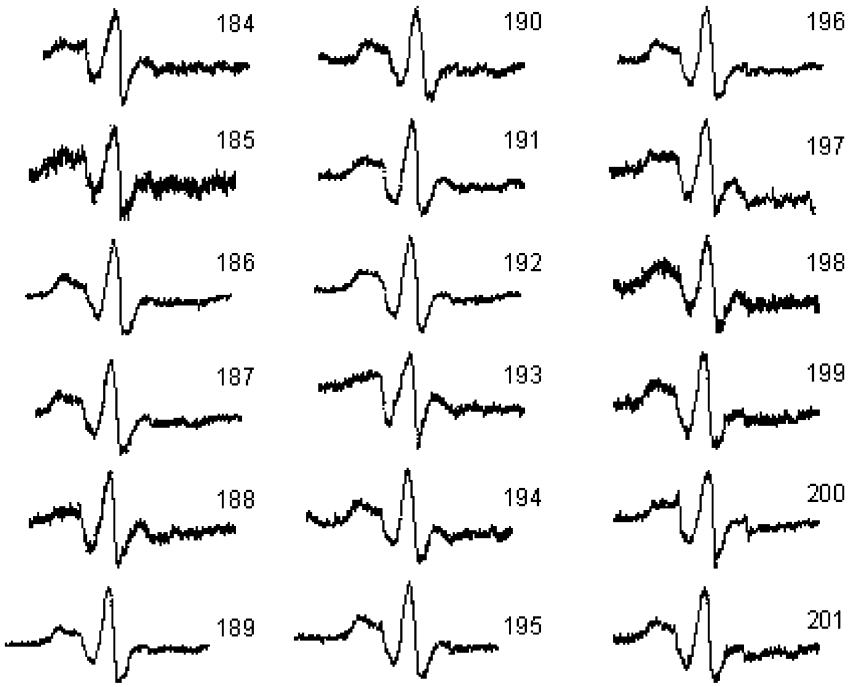

FIGURE 2: EPR spectra of single-Cys OGC mutants containing the nitroxide side chain at the indicated sites.

C-less value. The results indicate that the activity is negligible for the 184, 190, 191, and 198 mutants, while it is strongly reduced for 187 and 200. In agreement with these results, R190C and Q198C had previously been shown to be essential for transport and T187C and A191C to be strongly inactivated by *N*-ethylmaleimide or by methanethiosulfonate derivatives (*9*). The inactivation observed upon reaction of the spin-label with Cys184 (which is one of the three native OGC cysteines) may be due to the fact that this residue is important for the formation of a stable and functional dimeric protein (*5*), a process that may be hindered once cysteine 184 reacts with a bulky reagent such as MTSL. As regards the A200C mutant, inhibition had previously been observed upon reaction with MTSEA but not with MTSES and MTSET (*9*). Taken together, these results suggest that the A200C mutant may undergo different conformational changes depending on the chemical properties of the thiol reagent. Similarly, it is likely that mutants V194C and N195C also undergo different rearrangements according to the thiol reagent used, since they are almost completely inactivated by reaction with NEM (*9*) but are not substantially affected by the spin-label.

Mobility and Accessibility. Figure 2 shows the EPR spectra of the single-Cys 184−201 mutants labeled with MTSL. The structural analysis of the OGC TMSIV was based on individual line shape properties and on the determination of the collision frequencies obtained from power saturation experiments (*24*). The line shape of the spectra is a reporter of the local dynamics and of the local constraints affecting the nitroxide ring. In particular, measurements of the width of the central resonance line (ΔH), which is a parameter diagnostic of the mobility, can permit the identification of secondary structural elements when the investigated segment is not perturbed by interaction with other protein elements (*25, 26*). A semiquantitative analysis of the segment can be obtained by normalizing the inverse of the width of each signal's central resonance line to the scaled mobility Ms (*11*). Figure 3A, which reports Ms as a function of the label position along the 184−201 segment, indicates that this parameter has a clear oscillatory behavior, indicating a definite periodicity in the mobility of the attached label. Indeed, the experimental data follow a sinusoid with a period of 3.3, a value pretty close to that expected for an α-helix. Figure 3A also shows that TMSIV is characterized by two distinct regions with a significantly different average mobility. The C-terminal region (corresponding to three helix turns) has a low degree of mobility with a mean $M_s = 0.12$ typical of a highly packed helix, as found in bacteriorhodopsin (*11*). The mean scaled mobility in the N-terminal region of TMSIV (corresponding to two helix turns) is 0.23, a value that is higher than that calculated for the C-terminal region but still in the range characteristic of a relatively packed helix (*11*). Interestingly, the mobility break point occurs at residue 190, the position occupied in the native carrier by the arginine known to have a crucial role in the transport activity (*9, 27*). The difference in mobility between the N- and C-terminal parts of TMSIV suggests that the N-terminal part of the helix may undergo or be involved in a conformational change during transport. In agreement with this hypothesis, a substrate-induced change in the tertiary structure of OGC in this region has already been proposed to explain the enhanced binding of SH reagents to Cys184 in the presence of the carrier substrates (*10*).

Further information concerning the properties of the 184−201 segment can be obtained upon investigating the accessibility of the spin label to broadening reagents of different polarity. Two such reagents were used: molecular oxygen, which is highly soluble in the low dielectric lipid environment, and chromium oxalate (CrOx), which is a water-soluble Cr(III) chelate complex. Thus, high O_2 accessibility is diagnostic of a membrane-exposed residue, while high CrOx accessibility is indicative of a water-exposed residue. The accessibility parameters of the spin label bound to every single residue of the 184−201 segment were determined by

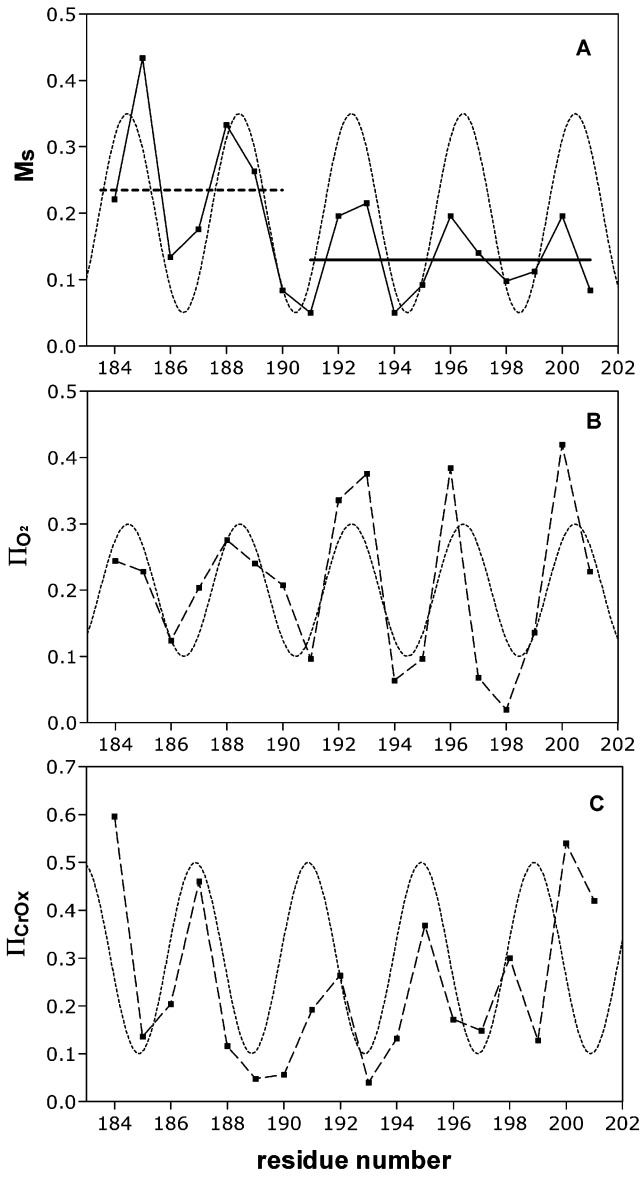

FIGURE 3: Residue-specific environmental parameter profiles for TMSIV: (A) Scaled mobility M_s as a function of residue number. The mean scaled mobilities for the N- and C-terminal parts are represented by a dashed and full line, respectively. (B) ΠO_2, accessibility to molecular oxygen; (C) ΠCrOx, accessibility to potassium chromium oxalate. In each panel the dotted line represents a sinusoid with a period of 3.3.

power saturation experiments carried out in the presence and absence of the two paramagnetic perturbing agents, as described in Materials and Methods. Typical power saturation curves for the label at position 197 are presented in Figure 4.

Figure 3B shows the plot of the O_2 accessibility profile (ΠO_2) along the 184−201 segment. ΠO_2 has a clear periodic behavior similar to that observed for the mobility parameter Ms, indicating low O_2 accessibility about every three residues. Again the data follow a sinusoid having a periodicity of about 3.3, which is in phase with the sinusoid overlapping the Ms data. The residues with the highest mobility correspond to local maxima in ΠO_2 as expected for residues that interface the lipid bilayer and do not interact with protein elements. Thus, these residues define one face of the helix which is solvated by the bilayer. It should be

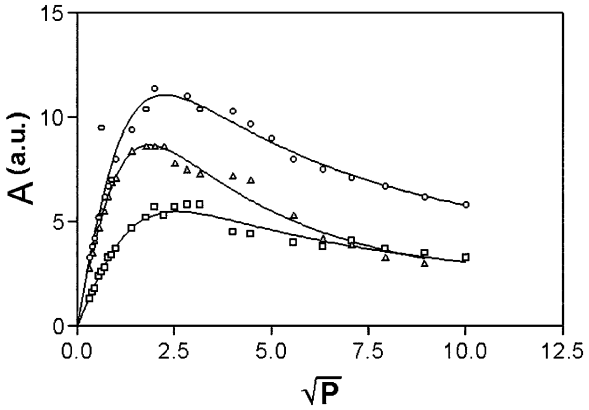

FIGURE 4: Power saturation curves for residue 197 of TMIV obtained from measurements under N_2 saturation (triangles), under O_2 saturation (circles), and under N_2 saturation in the presence of 30 mM CrOx (squares). The full lines represent the best fit of the signal amplitudes (*A*) measured at the indicated incident power as described in Materials and Methods. a.u., arbitrary units.

noted, however, that the ΠO_2 maximum values increase in the C-terminal part of the segment whereas the corresponding values of M_s decrease, indicating some steric constraints in this region of the protein.

The accessibility of the water-soluble CrOx along TMSIV displays a somewhat more complex behavior (Figure 3C). The ΠCrOx values oscillate quite sharply between maxima and minima, and they are not fitted so well by a sinusoid having a period of 3.3, particularly at the C-terminal extremity, as compared to the values of oxygen accessibility. TMSIV displays quite a high CrOx accessibility indicative of a relatively high collision probability (*28*, *29*). This can be explained, at least partly, by an electrostatic interaction between the negatively charged CrOx and the positive chain of Arg 190 (which is located in the middle of TMSIV in a water accessible environment (*9*)). In line with this hypothesis, the ΠCrOx value for position 190 (i.e., when Arg 190 residue is replaced with Cys) corresponds to a minimum of CrOx accessibility, supporting the idea that the presence of the charged guanidinium group plays an important role in determining the CrOx collision frequency. It has to be noted that the use of CrOx as a paramagnetic collision probe may cause some underestimation/overestimation of hydrophilic accessibility because of its charged character.

Helix Amphipaticity of TMSIV. Interestingly, the sinusoidal periodicity of ΠCrOx is out of phase with ΠO_2 (Figure 3B,C), indicating that TMSIV is an amphipatic helix. A direct way to identify faces of a transmembrane segment having polar or apolar character is to calculate the resultant vectors of the O_2 and CrOx accessibility values, as described in Materials and Methods, and to represent them on a helical wheel plot of the segment. Figure 5 shows that the resultant vectors of the O_2 and CrOx accessibility toward TMSIV of the OGC are opposite each other, forming an angle of more than 170°. This indicates that the hydrophobic and hydrophilic faces of TMSIV are opposite each other. Figure 5A also shows the mobility vector derived from the line width of the spectra. This vector has an orientation close to the resultant vector of the O_2 accessibility in agreement with the identification of the face of the helix exposed to lipids. On the other hand, the finding that the mobility vector is quite small suggests the existence of steric constraints,

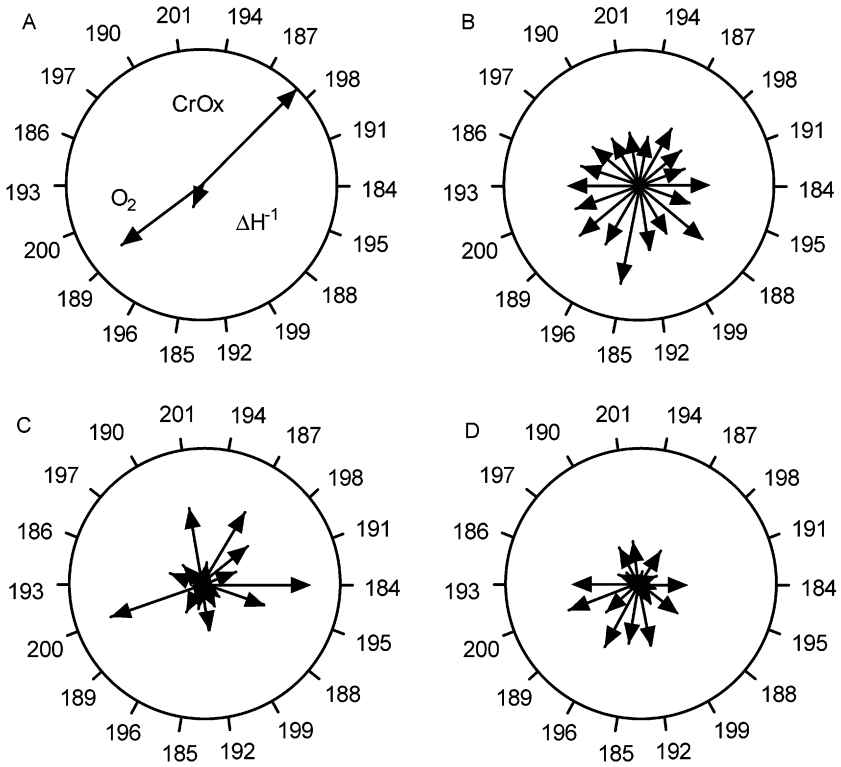

FIGURE 5: Helical wheel representation of TMSIV (from C184 to S201) showing the resultant vectors (panel A) and the individual vectors of the mobility parameter ΔH^{-1} (panel B), the CrOx accessibility (ΠCrOx, panel C), and the oxygen accessibility (ΠO_2, panel D). Wheel radii have been taken arbitrarily as 1 for panel A, 0.375 for panel B, and 0.75 for panels C and D.

particularly in the C-terminal half of the segment, which may be caused by interaction with other protein elements (*15*).

Topography of TMSIV. The CrOx accessibility plot displays a gradient of increasing accessibility which is almost symmetric from the center of the segment toward the extremities. This trend suggests that the carrier protein is randomly oriented into the reconstituted liposomes, thus permitting a higher CrOx collision frequency at both the C- and N-terminal regions of TMSIV. Information on the depth of a selected residue in the lipid bilayer can be provided by the parameter $\Phi = \ln(\Pi O_2/\Pi CrOx)$, which, for reagents of similar size and/or in the absence of structural constraints, mainly reflects the depth in the membrane (*24*). In principle, for a protein segment inserted in the membrane unidirectionally Φ should display a linear increase along the segment; for a segment inserted randomly Φ should show a behavior similar to an upturned V, i.e., exhibit a maximum in the middle of the segment. The Φ values calculated for the lipid-exposed residues of the OGC TMSIV, identified above by the ΠO_2 resultant vector in Figure 5A, increase from the extremities toward the center of the segment; i.e., the Φ plot versus residue numbers displays a trend of an upturned V with a maximum at position 193, corresponding to the center of the segment (Figure 6). This pattern is consistent with the random orientation of TMSIV in the membrane. The fact that the upturned V is quite broad may partly be explained by the lack of the expected increase in O_2 accessibility in the middle of the segment (Figure 3B). This lack may be accounted for by a close helix−helix interaction or by an interaction of helix IV with hydrophilic loops protruding into the membrane between the transmembrane segments. The helix−helix interaction may involve transmembrane segments of the same monomer or of the two subunits forming

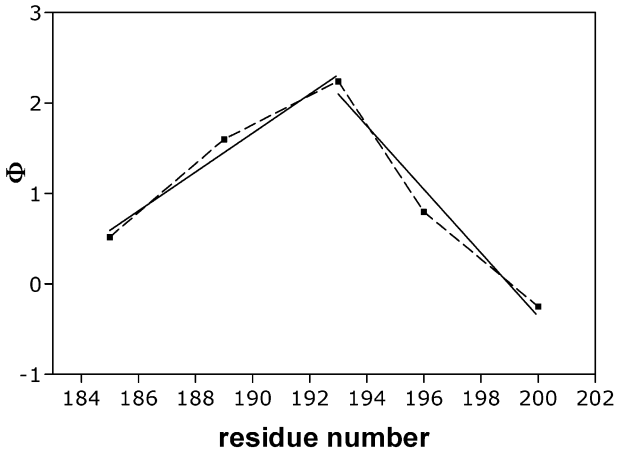

FIGURE 6: Depth parameter Φ of lipid-exposed spin-labeled residues along TMSIV. Linear regression of Φ values (from 185 to 193 and from 193 to 200) have been superimposed.

the dimeric structure of the carrier, in both cases producing a steric hindrance at the center of TMSIV of the oxoglutarate carrier. The possibility that residues of the hydrophilic loops closely interact with the residues located at the middle of TMSIV is in agreement with the proposals that hydrophilic loops of the ADP/ATP carrier, of the uncoupling protein, and of the carnitine/acylcarnitine carrier protrude from the matrix side into the membrane toward the outside between the transmembrane segments of these carriers (*30*−*34*). As a matter of fact, the OGC contains five charged residues in its putative transmembrane segments that are all positively charged and are all important for the transport function of this protein (*27*). It can be speculated that, in the absence of the carrier substrate, Arg 190 and possibly also the other intramembrane charged residues are compensated by nega-

tively charged residues present in the matrix hydrophilic loops.

To tackle the problem of the orientation of the recombinant OGC in the liposomal membrane directly, we investigated the ability of ASM, a fluorescent and highly impermeable thiol reagent (*35*, *36*), to interact with the single-Cys OGC mutants F208C and Y259C upon their reconstitution into liposomes. According to the folding model of OGC in the mitochondrial membrane (*7*), F208 is present in the hydrophilic loop connecting transmembrane segments IV and V, and Y259 in the hydrophilic loop between TMSV and TMSVI; i.e., F208 and Y259 are located on opposite sides of the membrane. Both F208C and Y259C, when reconstituted into liposomes under the experimental conditions used in the present study, react equally well with 20 μM ASM (data not shown). In contrast, ASM does not bind to the reconstituted C-less OGC, thus ruling out the possibility of any spurious protein-fluorescent reagent interaction. Therefore, the recombinant OGC mutants investigated here are randomly oriented into the proteoliposomal membrane.

CONCLUSIONS

The results presented here leave no room for doubt that the 184−201 segment of the OGC, believed to form the TMSIV of the carrier, has an α-helical conformation. They also indicate that this α-helix has a highly amphipatic character with a lipid-exposed face lying opposite a hydrophilic face which contains the essential residues R190 and Q198 and the residues found to be important by chemical modification. The present EPR data further support the idea that the hydrophilic face of TMSIV lines part of the translocation pathway through the OGC protein. In addition, the present work provides evidence for steric constraints mainly at the hydrophilic face but also at the level of the hydrophobic face, indicating a compact tertiary and/or quaternary structure around the OGC helix IV. Important issues such as the helix packing and helix-helix orientation within the dimeric structure of the OGC warrant further study. In future investigations, we plan to extend the site-directed spin labeling approach to other transmembrane segments of the OGC and determine the distances between pairs of engineered cysteines and/or between a tryptophan and a cysteine introduced in the protein at specific sites. For the first time we also obtained information on the dynamic properties displayed by a transmembrane segment of a mitochondrial carrier family member. On the basis of our mobility determinations, TMSIV appears to behave as a rigid body and therefore probably participates as a whole in the conformational changes accomplishing substrate translocation. Furthermore, the observation that the N-terminal part of the OGC TMSIV is comparatively less packed than the rest of the helix suggests that more pronounced rearrangements occur in or around this terminus. In this context we plan to further investigate the functional dynamics of the OGC protein in the presence of different substrates and inhibitors.

REFERENCES

1. Palmieri, F., Quagliariello, E., and Klingenberg, M. (1972) *Eur. J. Biochem. 29*, 408−416.
2. Kramer, R., and Palmieri, F. (1992) in *Molecular Mechanisms in Bioenergetics* (Ernster, L., Ed.) pp 359−384, Elsevier Science Publishers, Amsterdam.
3. Fiermonte, G., Palmieri, L., Todisco, S., Agrimi, G., Palmieri, F., and Walker, J. E. (2002) *J. Biol. Chem.* 277, 19289−19294.
4. Palmieri, F. (1994) *FEBS Lett. 346*, 48−54.
5. Bisaccia, F., Zara, V., Capobianco, L., Iacobazzi, V., Mazzeo, M., and Palmieri, F. (1996) *Biochim. Biophys. Acta 1292*, 281−288.
6. Runswick, M. J., Walker, J. E., Bisaccia, F., Iacobazzi, V., and Palmieri, F. (1990) *Biochemistry 29*, 11033−11040.
7. Bisaccia, F., Capobianco, L., Brandolin, G., and Palmieri, F. (1994) *Biochemistry 33*, 3705−3713.
8. Fiermonte, G., Walker, J. E., and Palmieri, F. (1993) *Biochem. J. 294*, 293−299.
9. Stipani, V., Cappello, A. R., Daddabbo, L., Natuzzi, D., Miniero, D. V., Stipani, I., and Palmieri, F. (2001) *Biochemistry 40*, 15805−15810.
10. Capobianco, L., Bisaccia, F., Mazzeo, M., and Palmieri, F. (1996) *Biochemistry 35*, 8974−8980.
11. Hubbell, W. L., Gross, A., Langen, R., and Lietzow, M. A. (1998) *Curr. Opin. Struct. Biol. 8*, 649−656.
12. Hubbell, W. L., Cafiso, D. S., and Altenbach, C. (2000) *Nat. Struct. Biol. 7*, 735−739.
13. Columbus, L., and Hubbell, W. L. (2002) *Trends Biochem. Sci. 27*, 288−295.
14. Altenbach, C., Klein-Seetharaman, J., Cai, K., Khorana, H. G., and Hubbell, W. L. (2001) *Biochemistry 40*, 15493−15500.
15. Perozo, E., Cortes, D. M., and Cuello, L. G. (1998) *Nat. Struct. Biol. 5*, 459−469.
16. Gross, A., Columbus, L., Hideg, K., Altenbach, C., and Hubbell, W. L. (1999) *Biochemistry 38*, 10324−10335.
17. Zhao, M., Zen, K. C., Hernandez-Borrell, J., Altenbach, C., Hubbell, W. L., and Kaback, H. R. (1999) *Biochemistry 38*, 15970−15977.
18. Kaplan, R. S., Mayor, J. A., Kotaria, R., Walters, D. E., and McHaourab, H. S. (2000) *Biochemistry 39*, 9157−9163.
19. Laemmli, U. K. (1970) *Nature (London) 227*, 680−685.
20. Palmieri, F., Indiveri, C., Bisaccia, F., and Iacobazzi, V. (1995) *Methods Enzymol. 260*, 349−69.
21. Phelps, A., Briggs, C., Mincone, L., and Wohlrab, H. (1996) *Biochemistry 35*, 10757−10762.
22. Farahbakhsh, Z. T., Altenbach, C., and Hubbell, W. L. (1992) *Photechem. Photobiol. 56*, 1019−033.
23. Wessel, D., and Flugge, U. I. (1984) *Anal. Biochem. 138*, 141−143.
24. Altenbach, C., Greenhalgh, D. A., Khorana, H. G., and Hubbell, W. L. (1994) *Proc. Natl. Acad. Sci. U.S.A. 91*, 1667−1671.
25. Mchaourab, H. S., Lietzow, M. A., Hideg, K., and Hubbell, W. L. (1996) *Biochemistry 35*, 7692−7704.
26. Altenbach, C., Yang, K., Farrens, D. L., Farahbakhsh, Z. T., Khorana, H. G., and Hubbell, W. L. (1996) *Biochemistry 35*, 12470−12478.
27. Palmieri, F., Bisaccia, F., Capobianco, L., Dolce, V., Fiermonte, G., Iacobazzi, V., Indiveri, C., and Palmieri, L. (1996) *Biochim. Biophys. Acta 1275*, 127−132.
28. Pfeiffer, M., Rink, T., Gerwert, K., Oesterhelt, D., and Steinhoff, H. J. (1999) *J. Mol. Biol. 287* (1), 163−171.
29. Wegener, C., Tebbe, S., Steinhoff, H. J., and Jung, H. (2000) *Biochemistry 39* (16), 4831−4837.
30. Bogner, W., Aquila, H., and Klingenberg, M. (1986) *Eur. J. Biochem. 161*, 611−620.
31. Mayinger, P., Winkler, E., and Klingenberg, M. (1989) *FEBS Lett. 244*, 421−426.
32. Majima, E., Ikawa, K., Takeda, M., Hashimoto, M., Shinohara, Y., and Terada, H. (1995) *J. Biol. Chem. 270*, 29548−29554.
33. Mayinger, P., and Klingenberg, M. (1992) *Biochemistry 31*, 10536−10543.
34. Indiveri, C., Giangregorio, N., Iacobazzi, V., and Palmieri, F. (2002) *Biochemistry 41*, 8649−8656.
35. Long, J. C., Wang, S., and Vik, S. B. (1998) *J. Biol. Chem. 273*, 16235−16240.
36. Bogdanov, M., Heacock, P. N., and Dowhan, W. (2002) *EMBO J. 21*, 2107−2116.

BI027025Q